




AgNWs-*a*-TiO_x: a scalable wire bar coated core–shell nanocomposite as transparent thin film electrode for flexible electronics applications

S. Arulkumar¹, T. Senthilkumar¹, S. Parthiban^{1,*} , Gnanaprakash Dharmalingam², Anandarup Goswami³, Saad M. Alshehri⁴, and Manoj B. Gawande^{5,6}

¹Advanced Materials and Devices Laboratory, PSG Institute of Advanced Studies, Coimbatore 641004, India

²Plasmonic Nanomaterials Laboratory, PSG Institute of Advanced Studies, Coimbatore 641004, India

³Division of Chemistry, Department of Sciences and Humanities, Vignan's Foundation for Science, Technology and Research (VFSTR), Vadlamudi, Guntur 522 213, Andhra Pradesh, India

⁴Department of Chemistry, College of Science, King Saud University, Riyadh 11451, Saudi Arabia

⁵Regional Centre of Advanced Technologies and Materials, Palacký University, Šlechtitelu 27, 783 71 Olomouc, Czech Republic

⁶Department of Industrial and Engineering Chemistry, Institute of Chemical Technology Mumbai-Marathwada Campus, Jalna, Maharashtra 431203, India

Received: 15 August 2020

Accepted: 18 January 2021

Published online:

8 February 2021

© The Author(s), under exclusive licence to Springer Science+Business Media, LLC part of Springer Nature 2021

ABSTRACT

Flexible electronic devices entail highly transparent and conducting electrodes with excellent adherent and mechanically robust properties along with excellent bendability. Here, we report the development of transparent and conducting electrodes comprising silver nanowires (AgNWs) and amorphous-titanium oxide (*a*-TiO_x) nanocomposite thin films. The AgNWs and *a*-TiO_x nanocomposite thin films were deposited by a wire bar coating process, a scalable and high throughput procedure. PXRD analysis confirmed the crystalline and amorphous nature for AgNWs and TiO_x thin film, respectively. FE-SEM and HRTEM analyses revealed the core–shell nature of the composite where AgNWs and *a*-TiO_x acted as core and shell, respectively. Even after three-layer coating of AgNWs-*a*-TiO_x nanocomposite thin films, high transparency (~ 77%) in the visible region (400–800 nm) and a sheet resistance of 23 Ω/sq were observed. Furthermore, tape peel off tests were conducted for AgNWs and AgNWs-*a*-TiO_x nanocomposite, which displayed high adherence for the three-layer coated AgNWs-*a*-TiO_x nanocomposite as compared with AgNWs alone. The formation of AgNWs-*a*-TiO_x core–shell structure enhances the intra-particle binding and network formation of AgNWs. The preliminary studies highlight that the developed AgNWs-*a*-TiO_x nanocomposite thin films have great potential as transparent electrodes for realizing scalable cost-effective flexible electronic devices.

Address correspondence to E-mail: parthimsc@gmail.com

1 Introduction

Flexible transparent electrodes (FTEs) have become a topic of considerable research interest as they are fast progressing to become an essential component for cost-effective organic-light-emitting diodes (OLEDs), touch screen, electrochromic windows, solar cells, etc. [1–3]. Apart from their high transparency and conductivity, FTEs are attractive due to its light weight, large-area coating possibilities, flexibility and high throughput manufacturing prospect to name a few [4–8]. Currently, sputtered indium-tin-oxide (ITO) coated thin films are extensively employed as transparent conducting oxide material in flexible devices [9]. However, the limited supply of indium (In) and its increasing demand from optoelectronic industry are restricting for the development of low-cost devices [10, 11]. In addition, in most of the cases, their mechanical stability worsens on repeated bending on flexible substrates which results into the loss of conductivity due to crack formation and brittleness [12]. In order to resolve the issue, other metal oxide-based composites such as aluminum-doped zinc oxide/ITO stacked layers have been used as transparent conducting oxide (TCO) thin films as alternatives to pristine ITO but the studies regarding their flexibility constraints did not offer the expected outcome [13]. Unlike oxide thin films, metallic nanowires have encouraging electrical and optical properties with an excellent flexibility [14]. Among the metallic nanowires the silver nanowires (AgNWs) are fascinating owing to high optical transparency ($\sim 90\%$), low resistance ($\sim 11 \Omega/\text{Sq}$) and excellent flexibility [15]. Notwithstanding, adhesion between a substrate and AgNWs remains a challenge for its practical applications as an integral component in FTEs [16–18]. Another major problem that limits the wider applicability of AgNWs in similar devices is its instability under oxidative environment as it increases the resistivity dramatically [19]. Several attempts have been made to improve the AgNWs adhesion to substrate and prevent oxidation [20–24]. Among them, sandwich structures composed of AgNWs film and a metal oxide and core-shell AgNWs-metal oxide layers have been suggested as promising methods to improve chemical stability as well as the adhesion (to the substrate) of AgNWs [25–29]. In that context, core-shell nanomaterials or nanocomposites offer unique advantage of combining the conducive properties of both core and shell to

achieve improved performance and stability as demonstrated by several examples in various fields including catalysis, drug delivery, biosensors and bio imaging, information storage and flexible electronics applications [30–39].

Though the combination of a metal oxide and AgNWs in a hybrid film facilitates effective charge carrier collection and acts as an electron/hole blocking layer for solar cells and OLED devices, it is important to develop a composite with high surface area using a combination of cost-effective metal oxide and AgNWs thin films for using in FTEs [40]. Unlike conventional vacuum processing techniques, solution processing technique is simple, low-cost, vacuum-free and can be done with high throughput [41]. Among the solution process techniques, wire bar and slot-die coating techniques have been demonstrated for the large-area coating applications with uniform and rapid processing [40, 42]. Typically, these techniques consume very less precursor ink solution compare to other techniques [41]. While these techniques have been employed to make large-area metal oxide and several research efforts have been made to coat uniform large-area AgNWs thin films on flexible substrates [42], an appropriate combination of these two concepts to prepare a composite for FTEs is yet to be established. This prompted us to develop a new approach for the fabrication of AgNWs-*a*-TiO_x transparent electrodes using sol-gel ink and roll-to-roll-processable wire bar coating. In our procedure, the metal oxide provides a protective encapsulation for AgNWs and improves adhesion to the substrate as well as the mechanical, and electrical stability.

2 Experimental section

Silver nanowires (AgNWs, 20 mg/mL in isopropanol) were purchased from Dycotech (DM-SNW-8001, United Kingdom) and used without further modifications for the fabrication of AgNWs transparent electrode. The average diameter of the AgNWs used was 35 nm and their average length was 60–120 μm . Titanium oxide (TiO_x) solution was prepared by following the previously reported process [43]. For the preparation of TiO_x, first the titanium precursor solution was prepared using 3 mL of titanium isopropoxide, 20 mL of 2-methoxyethanol and 1.2 mL of monoethanolamine. A 3-neck round bottom flask was heated at 120 °C with a flow of dry

Fig. 1 Schematic representation of bar coating process

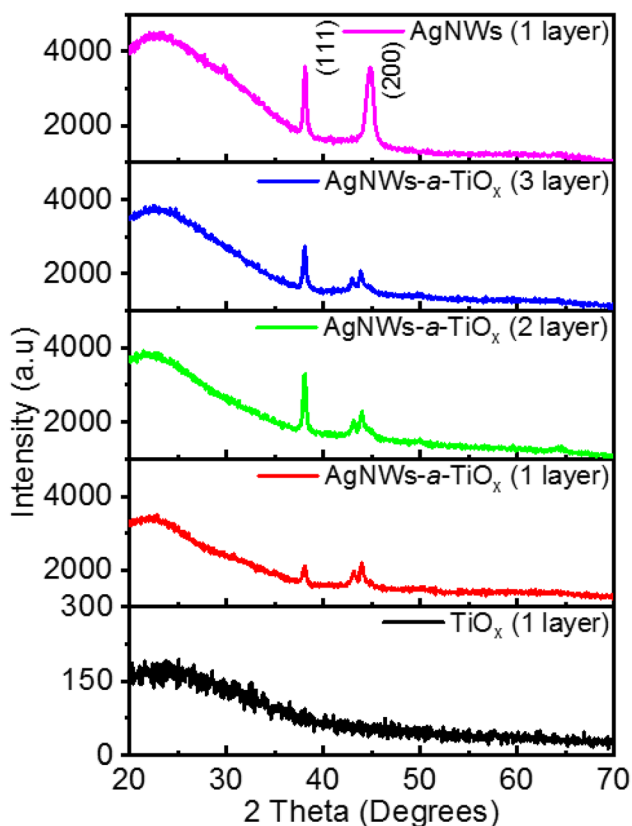
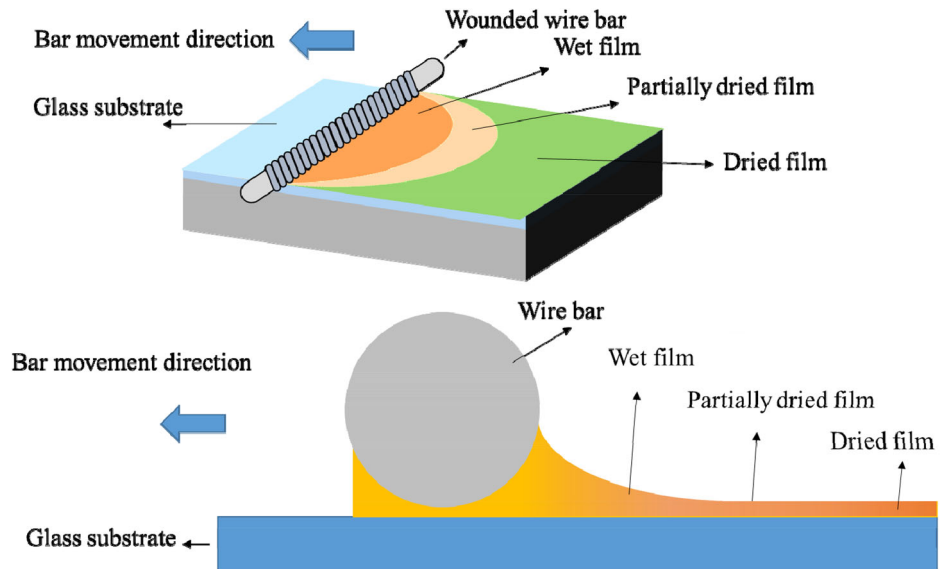


Fig. 2 XRD diffraction pattern of AgNWs, TiO_x and AgNWs- a - TiO_x nanocomposite thin films

N_2 for 1 h to remove atmospheric air and was allowed to cool at room temperature. Thereafter, the solutions were injected into the flask followed by stirring for 1 h at room temperature. The mixed

solution was heated for 1 h at 80 °C and for 1 h at 120 °C respectively and allowed to cool at room temperature. A 5 mL of methanol was injected to the solution and stirred for 10 min and extracted. The total volume was made-up to 20 mL by the addition of methanol to obtain a precursor solution with a concentration of 0.5 M. The prepared precursor solution was further diluted to 0.1 M using methanol. 150 μL of the synthesized TiO_x sol-gel (0.1 M) and 150 μL commercially purchased AgNWs ink solution were mixed well and was used for AgNWs and TiO_x composite thin film coating. The TiO_x sol-gel and AgNWs dispersion was stable and did not form any visible precipitation for more than 24 h.

Glass micro slides were cleaned by ultrasonication using distilled water, acetone and distilled water for 15 min each. The cleaned substrates were dried and subjected to UV (185 nm + 254 nm) treatment using PSDP UV8T for 10 min to remove organic residues. A 25 μL of solution containing AgNWs ink and TiO_x sol-gel was used for thin film deposition using a wire bar coater (RK print coater, United Kingdom). An 80 μm wire wound rod and a speed of 15 cm/s was utilized to deposit the nanocomposite thin films. The schematic representation of deposition of AgNWs- a - TiO_x nanocomposite thin film by bar coating process is depicted in Fig. 1. The wire bar coated AgNWs- a - TiO_x nanocomposite thin film was dried at 100 °C for 10 min to remove residual solvent.

The powder X-ray diffraction (PXRD) patterns were acquired using PANalytical Empereon with Cu-K_α radiation ($\lambda = 1.5418 \text{ \AA}$). High-resolution field

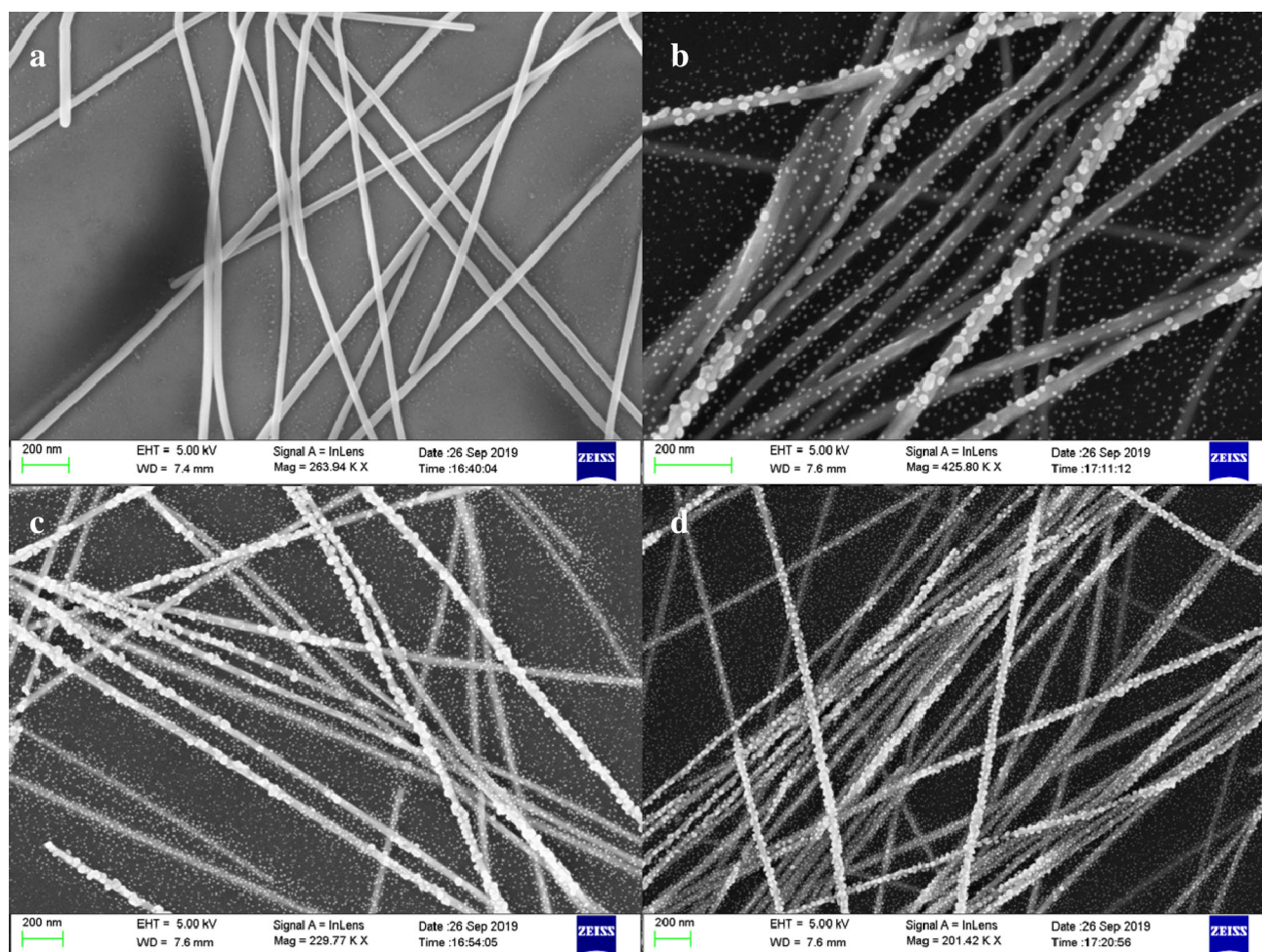


Fig. 3 FESEM image of **a** AgNWs, **b** 1 layer of AgNWs-*a*-TiO_x, **c** 2 layers of AgNWs-*a*-TiO_x and **d** 3 layers of AgNWs-*a*-TiO_x thin films

emission scanning electron microscope (FE-SEM) images were obtained using Carl Zeiss FE-SEM. Atomic Force Microscopy (AFM) scans were carried out using a NT-MDT system. Elemental compositions and the binding energies of the films were recorded using X-ray photoelectron spectroscopy (XPS) (Thermo scientific) with Al-K_α source. The images corresponding to High-resolution transmission electron microscopy (HRTEM) and selected area electron diffraction (SAED) were obtained using a JEOL JEM 2100 HRTEM. For transmission electron microscopy (TEM), the coated TiO_x thin film was removed from the glass substrate by gentle scratching, immersing it in ethanol solution and finally dropping a few drops of it on carbon coated copper grid, followed by drying in air. The transmittance spectra were measured using a double beam UV-Vis spectrophotometer (UV-1800 SHIMADZU). The identical glass substrates

were placed in the path of double beam for the baseline correction. The sample substrates were placed in the path of a sample beam side and measurements were carried out. The adhesion performance was measured by the Scotch tape peel testing using a motorized test stand system (ESM-303, Taber).

3 Results and discussion

The PXRD diffractogram of TiO_x thin film, AgNWs-*a*-TiO_x composite layers and AgNWs depicted in Fig. 2. Notably, TiO₂ polycrystalline anatase [44], rutile and brookite diffraction peaks were not observed in the XRD diffractogram of TiO_x thin film indicating the amorphous nature of the titania [45]. The peaks at 37.0° and 44.0° of AgNWs and AgNWs-*a*-TiO_x

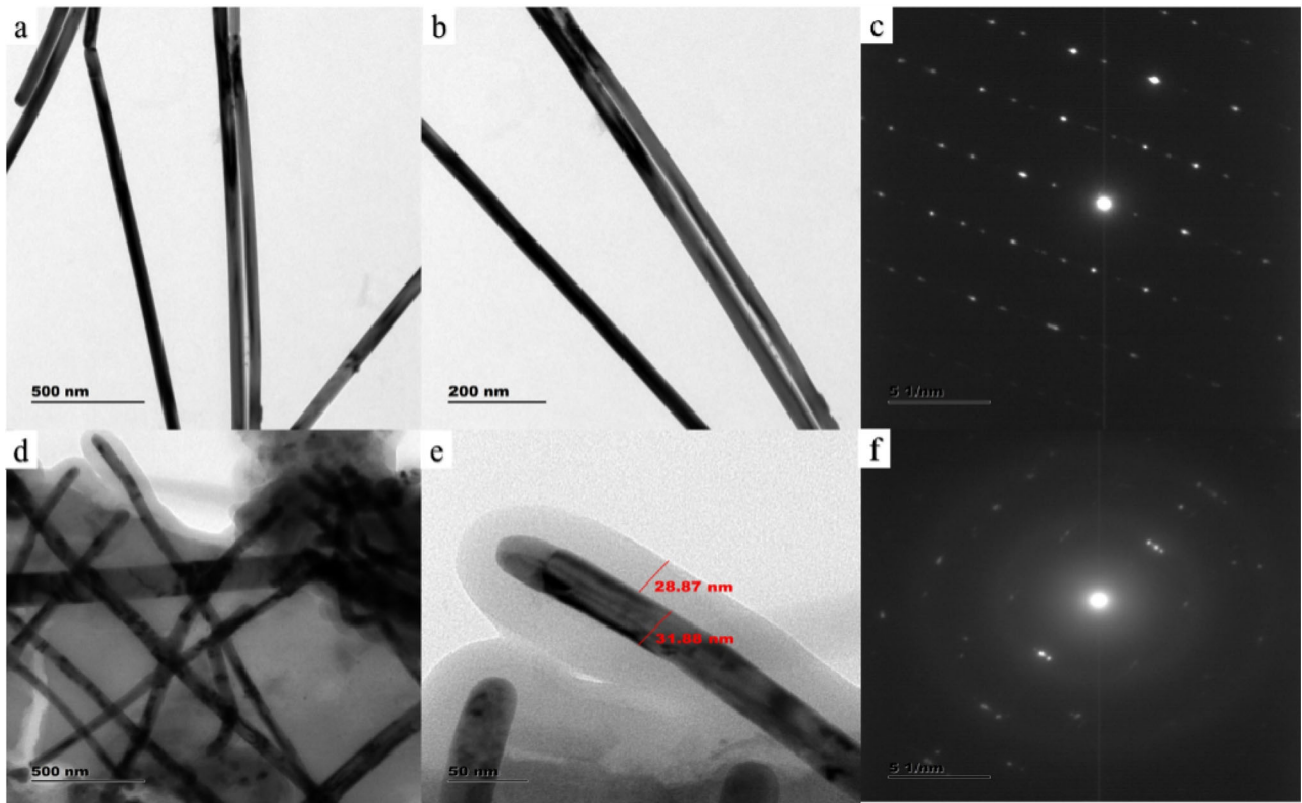


Fig. 4 HRTEM images of AgNWs (a, b) and 3 layers of AgNWs-*a*-TiO_x thin film (d, e). The SAED images of AgNWs (c) and 3 layers of AgNWs-*a*-TiO_x thin films (f) are also shown

composite layers correspond to the (111) and (200) crystal planes of silver nanoparticles [46]. The absence of any other characteristic diffraction peaks indicates that the composite layers contains Ag nanowire in the crystalline form and TiO_x in the amorphous state. The increase in the intensity of the characteristic diffraction peaks of Ag can presumably be attributed to the increase in density of AgNWs in the thin film as the number of layers was increased. The obtained diffraction peaks match well with previously reported solution processed AgNWs and AgNWs-*a*-TiO_x composite layers [25]. Figure 3a–d display the FESEM images of AgNWs and AgNWs-*a*-TiO_x composite layers formed on glass substrate by wire bar coating. The AgNWs have an average diameter of 35 nm, and is showing dense and cross-connected AgNWs network (Fig. 3a). Figure 3b–d show the FESEM images of AgNWs-*a*-TiO_x composite layers with respect to number of coating layers. These images clearly demonstrate the increase in the average diameter of AgNWs from 35 nm (pristine) to 43 nm (after 3 layers of deposition) indicating the

successful encapsulation of AgNWs by TiO_x layer. The images further display the presence of uneven TiO_x nanoparticles distributed on the glass surface and the surface of AgNWs. The presence of TiO_x nanoparticles in addition to the encapsulation of AgNWs by TiO_x layer was attributed to the agglomeration of excessive TiO_x solution during drying process. Figure 4a–f show HRTEM images of the AgNWs-*a*-TiO_x core-shell network which are similar to the previously reported results [25]. By comparing the SAED images of AgNWs and 3 layers of AgNWs-*a*-TiO_x thin film (Fig. 4c, f), a clear AgNWs crystalline structure can be seen for AgNWs-*a*-TiO_x thin films with the lattice spacing value of 0.24 nm corresponding to (111) planes of Ag [47], whereas the TiO_x shell on the nanowire exhibits amorphous structure. These results further confirm that the TiO_x thin layer covers the AgNWs and also further validates the results obtained from FE-SEM analysis. This is noteworthy, that no interface layer between AgNWs core and TiO_x shell was observed.

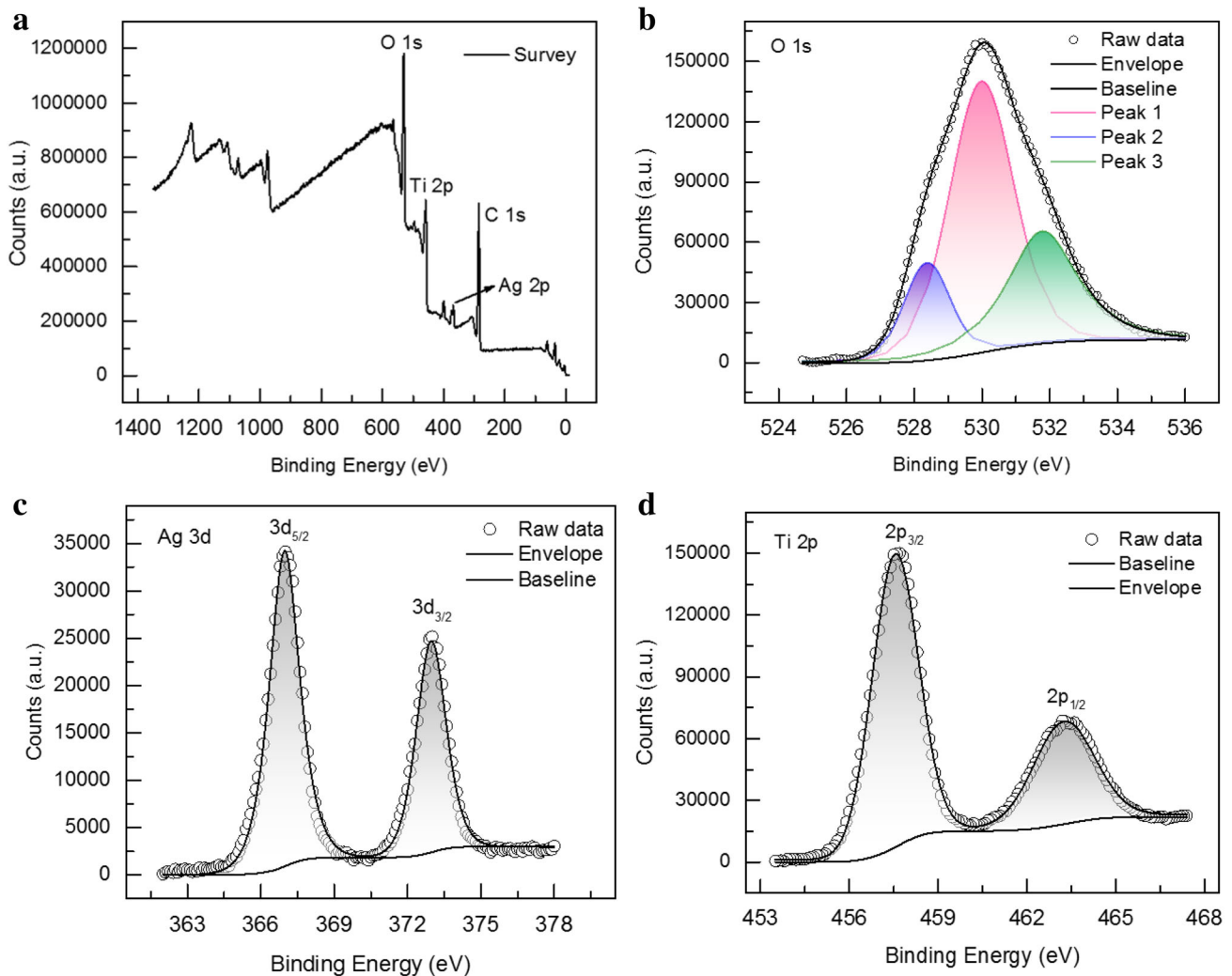


Fig. 5 **a** XPS spectra of AgNWs-*a*-TiO_x thin film, **b** O 1s spectra **c** Ag 3d spectra, and **d**) Ti 2p spectra

The elemental composition of AgNWs-*a*-TiO₂ thin film was obtained by XPS analysis and the acquired spectra indicates the presence of O, Ag and Ti in the sample. Figure 5 displays the XPS spectra of three-layer-coated AgNWs-*a*-TiO_x thin film. Ti 2p spectrum was analysed and the bands at 457.6 eV and 463.4 eV corresponds to the two spin-orbit doublets of 2p_{3/2} and 2p_{1/2} binding energies, respectively [48]. The Ag 3d spectrum was analysed and the bands at 367.0 eV and 373.0 eV correspond to the two spin-orbit doublets of 3d_{5/2} and 3d_{3/2} binding energies, respectively [49]. These spectra reveals the presence of Ti in +3 state and the reduction of Ti(IV)-precursors to Ti(+3) presumably proceeds via electron transfer from AgNWs as seen from the decrease in binding energy

of Ag [49]. Analysis of O 1s spectra reveals the presence of peak at 530.0 eV, which corresponds to O 1s orbit. The peak was deconvoluted into three sub-peaks where peak at 528.4 eV, 530.0 eV, and 531.7 eV correspond to lattice oxygen, metal oxide and metal hydroxide, respectively, supporting the absence of any undesired impurities in the sample [50, 51].

The atomic force microscopy images of AgNWs and AgNWs-*a*-TiO_x nanocomposite thin films were also obtained to compare the surface roughness of uncovered and TiO_x-covered AgNWs (Fig. 6). An average root mean square roughness of 24.08 nm was observed for pure AgNWs thin film. The average root mean square roughness of the AgNWs-*a*-TiO_x thin film increases from 10.93 to 16.09 nm with the

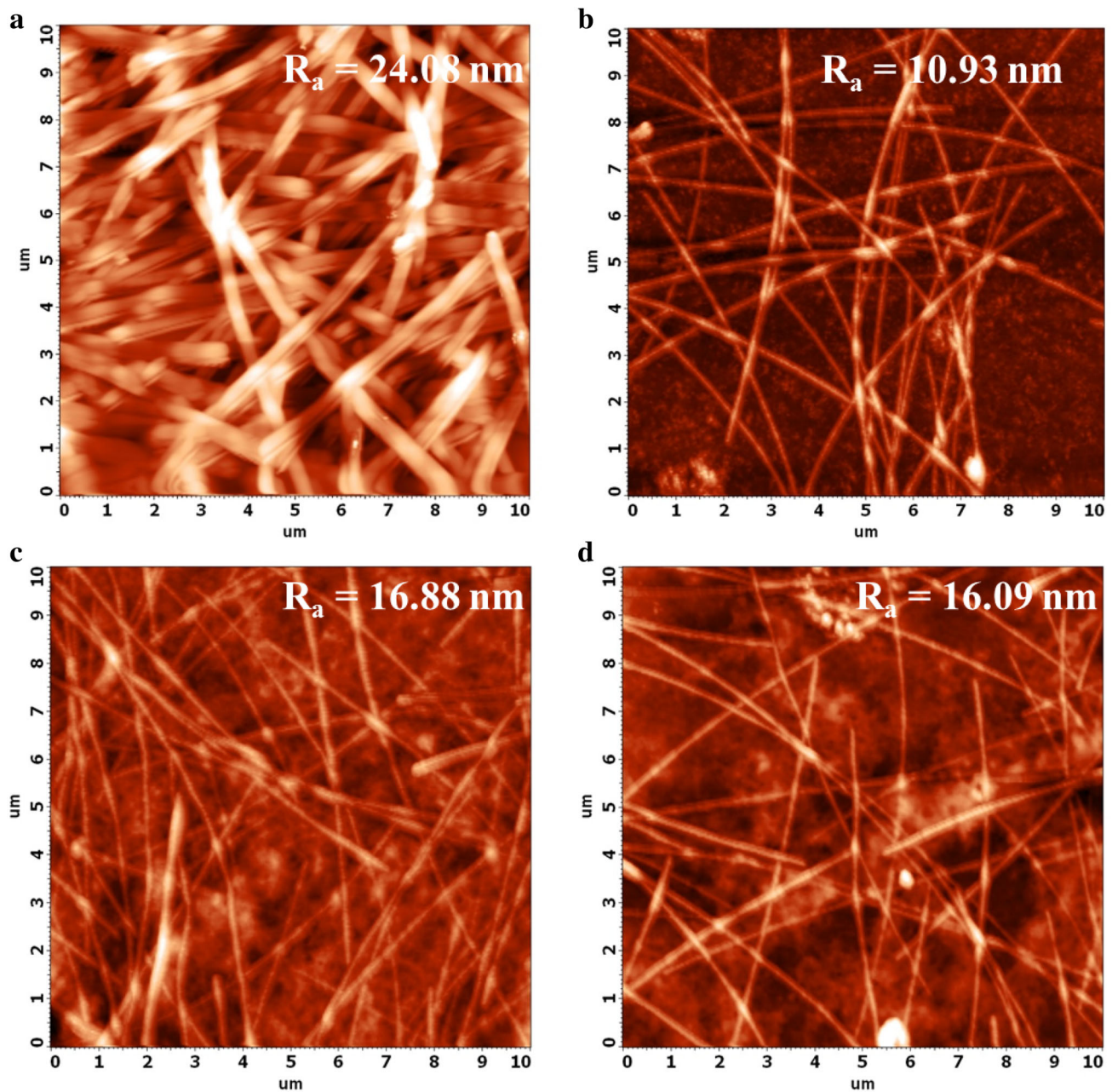


Fig. 6 Surface topography of **a** 1 layer of AgNWs **b** 1 layer of AgNWs-*a*-TiO_x, **c** 2 layers of AgNWs-*a*-TiO_x and **d** 3 layers of AgNWs-*a*-TiO_x thin films

increase in the number of layers of deposition from one to three layers, respectively. The formation of conductive networks by overlay and interlinking of Ag nanowires was also evident from the FE-SEM and AFM images of AgNWs-*a*-TiO_x thin film.

The optical and electrical properties of the multi-layered AgNWs-*a*-TiO_x thin films were compared with TiO_x thin film deposited using diluted TiO_x methanolic solution (0.1 M). AgNWs thin films were deposited using as-purchased AgNWs ink as well as with the solution containing AgNWs diluted with

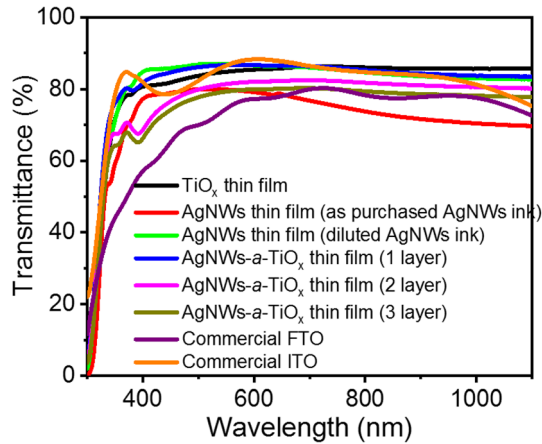


Fig. 7 Transmittance spectra of samples coated with AgNWs-*a*-TiO_x of 1 layer, 2 layer and 3 layer, AgNWs, TiO_x, commercial FTO and ITO

equal volume of methanol on glass substrates, respectively. The obtained results were compared with commercially purchased ITO (Sigma, 578,274) and FTO (Sigma, 735,167) coated glass substrates. Figure 7 shows the transmittance spectra of AgNWs, TiO_x thin film and AgNWs-*a*-TiO_x composite layers, as well as for commercial ITO and FTO glass substrates. The average visible transmittance of 72.8% was observed for AgNWs coated glass substrate deposited using as-purchased AgNWs ink which is on par with commercial FTO coated glass substrates

whereas the average visible transmittance of glass substrate coated with diluted AgNWs ink is 81% which is on par with commercial ITO coated glass substrates. The average visible transmittances of AgNWs-*a*-TiO_x composite thin films are higher than AgNWs deposited using as-purchased AgNWs ink owing to decrease in AgNW content as seen between as-purchased and diluted AgNW film, respectively. The average visible transmittance of AgNWs and AgNWs-*a*-TiO_x with respect to coating layer is shown in Table 1. The average transmittance of one layer of AgNWs-*a*-TiO_x thin film on glass substrate was 85.7%, which decreased with upon on the deposition of consequent AgNWs-*a*-TiO_x layers. However, the obtained transmittance of AgNWs-*a*-TiO_x composite thin film was still higher than AgNWs deposited using as-purchased AgNWs ink and commercial FTO coated glass substrates. The three-layer coated AgNWs-*a*-TiO_x composite layers exhibited 77% transparency in the visible region of 400–800 nm. These results indicate that the concentration of AgNWs on the thin film was a major factor affecting the visible transmittance and three-layer coated AgNWs-*a*-TiO_x composite layer has lower density of AgNWs than AgNW thin film deposited using as-purchased AgNWs ink. The extracted transmittance values are listed in Table 1.

The sheet resistance of the thin films coated on glass substrates were investigated by Hall measurements using Van der Pauw method (HMS 5000,

Table 1 Optical and electrical properties of AgNWs and AgNWs-*a*-TiO_x nanocomposite layers

Material	Average transparency in the visible region (400- 800 nm) T (%)	Sheet resistance before peel-off test (Ω/sq)	Sheet resistance after peel-off test (Ω/sq)
TiO _x thin film	84.3	29,980	30,285
AgNWs thin film (as-purchased AgNWs ink)	72.8	30.8	4032.1
AgNWs thin film (diluted AgNWs ink)	85.1	2898	–
AgNWs- <i>a</i> -TiO _x thin film (1 layer)	85.7	138.65	144.4
AgNWs- <i>a</i> -TiO _x thin film (2 layer)	79.8	29.1	28.9
AgNWs- <i>a</i> -TiO _x thin film (3 layer)	77.5	23.7	23.8
Commercial FTO	72.9	29.8	29.9
Commercial ITO	86.4	17.0	17.3

ECOPIA). A conducting silver paste was applied on the four corners of sample. Four spring loaded tips were used to make contact instead of using bonding wires on the sample corners. Sample perimeter of four sides of resistance values were measured by applying current through two terminals and measuring the voltage across the two terminals. In total four different resistance values were measured. The applied current was fixed in the range between -5 mA and 5 mA for all the measurements. The resistance is generally defined as $R_{ab,cd} = V_{cd}/I_{ab}$, where a , b , c and d are integers corresponding to terminals 1 through 4. The average of the four values is defined as R_s . The sheet resistance of AgNWs film deposited using AgNWs ink was found to be $30.8 \Omega/\text{sq}$ on average. The sheet resistance of AgNWs- a -TiO_x composite layers decreases with increasing number of layers owing to increase in the number of AgNWs (Table 1). The lowest sheet resistance was found to be $23.7 \Omega/\text{sq}$ for three-layer-coated AgNWs- a -TiO_x composite film. Further, it has to be noted that the sheet resistance of AgNWs thin film deposited using diluted AgNWs ink was tenfolds greater than single layer coated AgNWs- a -TiO_x thin film. This shows that presence of TiO_x thin film increases the binding between AgNWs and improves the conductive network formation. Tape peel-off test was carried out and the sheet resistance of three-layered AgNWs- a -TiO_x composite film was found to be same whereas the sheet resistance of AgNWs thin film deposited using as-purchased AgNWs ink increased by more than 100-folds. This confirms the improved adhesivity of the AgNWs- a -TiO_x composite film compared with AgNWs thin film [25].

4 Conclusion

Highly transparent electrodes, prepared from AgNWs- a -TiO_x thin film of comparable performance to conventionally deposited conducting thin films, were deposited on glass substrates via a simple, low-cost solution process using bar coater. The presence of Ag, Ti and O was confirmed by XPS analysis and the phase purity of AgNWs and amorphous nature of TiO_x were confirmed by XRD analysis. FE-SEM and HRTEM analysis revealed the formation of a core-shell structure of the film, where AgNWs core is covered with TiO_x thin film. The density of AgNWs- a -TiO_x thin films increased by increasing the number

of layers of deposition. The coated thin film exhibited low resistance of $24 \Omega/\text{sq}$ with an optical transparency of 77%. The tape peel-off test confirmed the high adhesivity of the thin film for three layers of AgNWs- a -TiO_x coating. These findings clearly indicate that the coatings (presented here as well as synthesized using related methods and precursors) have great potential to be employed as electrodes for flexible device fabrication applications.

Acknowledgements

The authors are thankful to the Department of Science and Technology-Science and Engineering Research Board, Government of India for financial support under the early career research award (File No. ECR/2016/000785). The author (SMA) thanks to Researchers Supporting Project number (RSP-2020/29), King Saud University, Riyadh, Saudi Arabia. The author T. S. is thankful to PSG Son's and Charities Fellowship for providing financial support.

Compliance with ethical standards

Conflict of interest The authors declare no conflict of interest.

References

1. A. Kim, Y. Won, K. Woo, C.H. Kim, J. Moon, ACS Nano 7, 1081–1091 (2013). <https://doi.org/10.1021/nn305491x>
2. Y. Wang, P. Liu, H. Wang, B. Zeng, J. Wang, F. Chi, J. Mater. Sci. 54, 2343–2350 (2019). <https://doi.org/10.1007/s10853-018-2986-9>
3. S. Chen, Y. Guan, Y. Li, X. Yan, H. Ni, L. Li, J. Mater. Chem. C 5, 2404–2414 (2017). <https://doi.org/10.1039/C6TC05000J>
4. S. Cho, S. Kang, A. Pandya, R. Shanker, Z. Khan, Y. Lee, J. Park, S.L. Craig, H. Ko, ACS Nano 11, 4346–4357 (2017). <https://doi.org/10.1021/acsnano.7b01714>
5. C. Lee, Y. Oh, I.S. Yoon, S.H. Kim, B.K. Ju, J.M. Hong, Sci. Rep. 8, 2763 (2018). <https://doi.org/10.1038/s41598-018-20368-3>
6. H. Gu, C. Guo, S. Zhang, L. Bi, T. Li, T. Sun, S. Liu, ACS Nano 12, 559–567 (2018). <https://doi.org/10.1021/acsnano.7b07360>
7. D.J. Lee, Y. Oh, J.M. Hong, Y.W. Park, B.K. Ju, Sci. Rep. 8, 14170 (2018). <https://doi.org/10.1038/s41598-018-32590-0>

8. B.H. Bae, S. Jun, M.S. Kwon, Y.W. Park, C.J. Han, S. Kim, B.K. Ju, *Opt. Mater.* **92**, 87–94 (2019). <https://doi.org/10.1016/j.optmat.2019.04.007>
9. H. Liu, V. Aurutin, N. Izyumskaya, U. Ozgur, H. Morkoc, *Superlattices Microstruct.* **48**, 458–484 (2010). <https://doi.org/10.1016/j.spmi.2010.08.011>
10. M. Loknac, R. Eggert, M. Redlinger, The availability of Indium: the present, medium term, and long term, National Renewable Laboratory (NREL), USA. <https://www.nrel.gov/docs/fy16osti/62409.pdf>
11. S.C. Dixon, D.O. Scanlon, C.J. Carmalt, I.P. Parkin, *J. Mater. Chem. C* **4**, 6946 (2016). <https://doi.org/10.1039/C6TC01881E>
12. D.P. Tran, H. Lu, C.K. Lin, *Coatings* **8**, 212 (2016). <https://doi.org/10.3390/coatings8060212>
13. X. Shen, M. Yang, C. Zhang, Z. Qiao, H. Wang, C. Tang, *Superlattices Microstruct.* **123**, 251–256 (2018). <https://doi.org/10.1016/j.spmi.2018.09.001>
14. T. Sannicolo, M. Lagrange, A. Cabos, C. Celle, J.P. Simonato, D. Bellet, *Small* **12**, 6052–6075 (2016). <https://doi.org/10.1002/sml.201602581>
15. S. Coskun, E.S. Ates, H.E. Unalan, *Nanotechnology* **24**, 125202 (2013). <https://doi.org/10.1088/0957-4484/24/12/125202>
16. B. Zheng, Q. Zhu, Y. Zhao, *J. Mater. Sci.* **54**, 5802–5812 (2019). <https://doi.org/10.1007/s10853-018-03235-4>
17. M.X. Jing, M. Li, C.Y. Chen, Z. Wang, X.Q. Shen, *J. Mater. Sci.* **50**, 6437–6443 (2015). <https://doi.org/10.1007/s10853-015-9198-3>
18. Y. Tao, D. Pan, *Mater. Res. Express* **6**, 076430 (2019). <https://doi.org/10.1088/2053-1591/ab17a4>
19. B.T. Liu, S.X. Huang, *RSC Adv.* **4**, 59226–59232 (2014). <https://doi.org/10.1039/C4RA11660G>
20. L. Miao, G. Liu, K. McEleney, J. Wang, *J. Mater. Sci.* **54**, 10355–10370 (2019). <https://doi.org/10.1007/s10853-019-03507-7>
21. S. Kim, S.Y. Kim, M.H. Chung, J. Kim, J.H. Kim, *J. Mater. Chem. C* **3**, 5859–5868 (2015). <https://doi.org/10.1039/C5TC00801H>
22. P. Kumar, F. Shahzad, S.M. Hong, C.M. Koo, *RSC Adv.* **6**, 101283–101287 (2016). <https://doi.org/10.1039/C6RA18652A>
23. F. Alotaibi, T.T. Tuang, M.J. Nine, C.J. Coghlan, D. Losic, *A.C.S. Appl. Nano Mater.* **1**, 2249–2260 (2018). <https://doi.org/10.1021/acsnm.8b00255>
24. M.C. Han, H.W. He, B. Zhang, X.X. Wang, J. Zhang, M.H. You, S.Y. Yan, Y.Z. Long, *Mater. Res. Express* **4**, 075043 (2017). <https://doi.org/10.1088/2053-1591/aa7c13>
25. Y. Huang, Y. Tian, C. Hang, Y. Liu, S. Wang, M. Qi, H. Zhang, Q. Peng, *A.C.S. Appl. Nano Mater.* **2**, 2456–2466 (2019). <https://doi.org/10.1021/acsnm.9b00337>
26. X. Zhang, J. Wu, J. Wang, Q. Yang, B. Zhang, Z. Xie, *A.C.S. Appl. Mater. Interfaces* **8**, 34630–34637 (2016). <https://doi.org/10.1021/acsnm.6b11978>
27. E. Lee, J. Ahn, H.C. Kwon, S. Ma, K. Kim, S. Yun, J. Moon, *Adv. Energy Mater.* **8**, 1702182 (2018). <https://doi.org/10.1002/aenm.201702182>
28. A. Kim, Y. Won, K. Woo, S. Jeong, J. Moon, *Adv. Funct. Mater.* **24**, 2462–2471 (2014). <https://doi.org/10.1002/adfm.201303518>
29. M. Singh, P. Prasher, J. Kim, *Nano-Structured & Nano-Objects* **16**, 151–155 (2018). <https://doi.org/10.1016/j.nanoso.2018.05.009>
30. M.B. Gawande, A. Goswami, T. Asefa, H. Guo, A.V. Biradar, D.L. Peng, R. Zboril, R.S. Varma, *Chem. Soc. Rev.* **44**, 7540–7590 (2015). <https://doi.org/10.1039/C5CS00343A>
31. Y. Hou, Y. Liu, R. Gao, Q. Li, H. Guo, A. Goswami, R. Zboril, M.B. Gawande, X. Zou, *ACS Catal.* **7**, 7038–7042 (2017). <https://doi.org/10.1021/acscatal.7b02341>
32. A. Goswami, A.K. Rathi, C. Aparicio, O. Tomanec, M. Petr, R. Pocklanova, M.B. Gawande, R.S. Varma, R. Zboril, *A.C.S. Appl. Mater. Interfaces* **9**, 2815–2824 (2017). <https://doi.org/10.1021/acsnm.6b13138>
33. A.K. Rathi, H. Kmentová, A. Naldoni, A. Goswami, M.B. Gawande, R.S. Varma, S. Kment, R. Zboril, *ACS Appl. Nano Mater.* **1**, 2526–2535 (2018). <https://doi.org/10.1021/acsnm.8b00078>
34. V.C. Anitha, A. Goswami, H. Sopha, D. Nandan, M.B. Gawande, K. Cepe, S. Ng, R. Zboril, J.M. Macak, *Appl. Mater. Today* **10**, 86–92 (2018). <https://doi.org/10.1016/j.apmt.2017.12.006>
35. S. Panimalar, R. Uthrakumar, E. TamilSelvi, P. Gomathy, C. Inmozhi, K. Kaviyarasu, J. Kennedy, *Surf. Interfaces* **20**, 100512 (2020). <https://doi.org/10.1016/j.surf.2020.100512>
36. K. Kaviyarasu, C. Maria Magdalane, D. Jayakumar, Y. Samson, A.K.H. Bashir, M. Maaza, D. Letsholathebe, A.H. Mahmoud, J. Kennedy, *J. King Saud Uni. Sci.* **32**, 1516–1522 (2020). <https://doi.org/10.1016/j.jksus.2019.12.006>
37. Y. Wang, L.T. Tseng, P.P. Murmu, N. Bao, J. Kennedy, M. Ionesc, J. Ding, K. Suzuki, S. Li, J. Yi, *Mater. Des.* **121**, 77–84 (2017). <https://doi.org/10.1016/j.matdes.2017.02.037>
38. K. Kasinathan, J. Kennedy, M. Elayaperumal, M. Henini, M. Malik, *Sci. Rep.* **6**, 38064 (2016). <https://doi.org/10.1038/srep38064>
39. M.C. Mbambo, S. Khamlich, T. Khamliche, M.K. Moodley, K. Kaviyarasu, I.G. Madiba, M.J. Madito, M. Khenfouch, J. Kennedy, M. Henini, E. Manikandan, M. Maaza, *Sci. Rep.*

- 10, 10982 (2020). <https://doi.org/10.1038/s41598-020-67418-3>
40. J. Wang, M. Liang, Y. Fang, T. Qiu, J. Zhang, L. Zhi, *Adv. Mater.* **24**, 2874 (2012). <https://doi.org/10.1002/adma.201200055>
41. W.J. Lee, W.T. Park, S. Park, S. Sung, Y.Y. Noh, M.H. Yoon, *Adv. Mater.* **27**, 5043–5048 (2015). <https://doi.org/10.1002/adma.201502239>
42. D.J. Kim, H.I. Shin, E.H. Ko, K.H. Kim, T.W. Kim, H.K. Kim, *Sci. Rep.* **6**, 34322 (2016). <https://doi.org/10.1038/srep34322>
43. S. Cho, K. Lee, A.J. Heeger, *Adv. Mater.* **21**, 1941 (2009). <https://doi.org/10.1002/adma.200803013>
44. P. Divya, S. Arulkumar, S. Parthiban, A. Goswami, T. Ahmad, M.B. Gawande, *Molecules* **25**, 1683 (2020). <https://doi.org/10.3390/molecules25071683>
45. S. Arulkumar, S. Parthiban, A. Goswami, R.S. Varma, M. Naushad, M.B. Gawande, *Mater. Res. Express* **6**, 126427 (2019). <https://doi.org/10.1088/2053-1591/ab5eed>
46. X. Xia, B. Yang, X. Zhang, C. Zhou, *Mater. Res. Express* **2**, 075009 (2015). <https://doi.org/10.1088/2053-1591/2/7/075009>
47. Z. Nengduo, Y. Xuesonga, G. Hao, *RSC Adv.* **6**, 47552–47561 (2016). <https://doi.org/10.1039/C6RA05448J>
48. M. Hannula, H. Ali-Löyty, K. Lahtonen, E. Sarlin, J. Saari, M. Valden, *Chem. Mater.* **30**, 1199–1208 (2018). <https://doi.org/10.1021/acs.chemmater.7b02938>
49. P. Ramasamy, D.M. Seo, S.H. Kim, J. Kim, *J. Mater. Chem.* **22**, 11651–11657 (2012). <https://doi.org/10.1039/C2JM00010E>
50. J.L.G. Fierro, M.A. Peña, L.G. Tejuca, *J. Mater. Sci.* **23**, 1018–1023 (1988). <https://doi.org/10.1007/BF01154005>
51. S.J. Yuan, F.J. Xu, S.O. Pehkonen, Y.P. Ting, E.T. Kang, K.G. Neoh, *J. Electrochem. Soc.* **155**, C196–C210 (2008). <https://doi.org/10.1149/1.2885073>

Publisher's Note Springer Nature remains neutral with regard to jurisdictional claims in published maps and institutional affiliations.